

## Research Article

# Efficient Continuation Methods for Computing Ground States of Quasi-2D Rotating Dipolar Bose-Einstein Condensates

B.-W. Jeng<sup>1</sup>, P.-H. Su,<sup>2</sup> and M.-I. Char<sup>2</sup>

<sup>1</sup>Department of Mathematics Education, National Taichung University of Education, Taichung 403, Taiwan

<sup>2</sup>Department of Applied Mathematics, National Chung Hsing University, Taichung 402, Taiwan

Correspondence should be addressed to B.-W. Jeng; bwjeng@mail.ntcu.edu.tw

Received 19 November 2021; Revised 1 July 2022; Accepted 5 July 2022; Published 4 August 2022

Academic Editor: Ruben Specogna

Copyright © 2022 B.-W. Jeng et al. This is an open access article distributed under the Creative Commons Attribution License, which permits unrestricted use, distribution, and reproduction in any medium, provided the original work is properly cited.

We study efficient continuation methods for computing the ground state solution of quasi-2D rotating dipolar Bose-Einstein condensates (BECs). First, the highly accurate spectral collocation method is used to discretize the governing Gross-Pitaevskii equation (GPE). Then, we modify the two-level continuation scheme for 3D dipolar BECs described in Jeng et al. (2014) to develop a single-parameter continuation method for quasi-2D rotating dipolar BECs, where the chemical potential is treated as the continuation parameter. Further, by adding the ratio of dipolar interaction strength to contact interaction strength as the second continuation parameter, we propose an efficient two-parameter continuation method which can effectively show the change of the ground-state vortex structures as the dipolar interaction strength gradually increases. Moreover, we also study linear stability analysis for the GPE. Sample numerical results on quasi-2D rotating dipolar BECs are reported.

## 1. Introduction

In 2005, the first dipolar Bose-Einstein condensate (BEC) was successfully produced by the group of Griesmaier [1] at the University of Stuttgart, in a gas of  $^{52}\text{Cr}$  atoms cooled to 700 nK. Later in 2011, Lu et al. [2] at Stanford University realized a dipolar BEC of  $^{164}\text{Dy}$  atoms. The next year, a dipolar BEC of  $^{168}\text{Er}$  atoms was also achieved in experiments at Innsbruck University [3]. These successful experiments provided new impetus for the theoretical and numerical studies of dipolar BECs.

In dipolar BECs, since  $^{52}\text{Cr}$ ,  $^{168}\text{Er}$ , and  $^{164}\text{Dy}$  atoms have larger magnetic moments, the long-range dipolar interaction is nonnegligible, and it induces various interesting phenomena such as  $d$ -wave collapse and expansion [4], roton spectrum [5, 6], self-bound dipolar droplets [7, 8], and the supersolid phase [9]. Moreover, vortices are also an important topic in BECs, which can be created by rotating the trap. In this paper, we will develop efficient numerical methods for computing the ground state solution of rotating dipolar BECs and then investigate the ground-state vortex structures.

Using the mean-field theory, the three-dimensional (3D) rotating dipolar BEC at absolute zero temperature is well

described by the macroscopic wave function  $\Psi(\mathbf{x}, t)$  whose evolution is governed by the dimensionless Gross-Pitaevskii equation (GPE) [10–12].

$$i\partial_t\Psi(\mathbf{x}, t) = \left[ -\frac{1}{2}\Delta + V(\mathbf{x}) + \beta|\Psi|^2 + \lambda(U_{\text{dip}}(\mathbf{x}) * |\Psi|^2) - \omega L_z \right] \Psi(\mathbf{x}, t), \mathbf{x} \in \mathbb{R}^3, t > 0, \quad (1)$$

where  $i = \sqrt{-1}$  is the imaginary unit;  $\mathbf{x} = (x, y, z)$  is the spatial variable;  $t$  is the time variable;  $*$  denotes the convolution operator with respect to the spatial variable;  $V(\mathbf{x}) = (1/2)(\gamma_x^2 x^2 + \gamma_y^2 y^2 + \gamma_z^2 z^2)$  is the harmonic trapping potential with  $\gamma_x$ ,  $\gamma_y$ , and  $\gamma_z$  being the trap frequencies in the  $x$ -,  $y$ -, and  $z$ -direction, respectively;  $\beta$  and  $\lambda$  are constants representing the strength of the contact (or short-range) and dipolar (or long-range) interaction, respectively;  $U_{\text{dip}}(\mathbf{x}) = (3/4\pi)(1 - 3(\mathbf{x} \cdot \mathbf{n})^2/|\mathbf{x}|^2)/|\mathbf{x}|^3$  is the long-range dipolar interaction potential with the dipolar axis  $\mathbf{n} = (n_1, n_2, n_3) \in \mathbb{R}^3$  satisfying  $|\mathbf{n}| = \sqrt{n_1^2 + n_2^2 + n_3^2} = 1$ ;  $\omega$  is angular velocity of the laser beam; and  $L_z = xp_y - yp_x = -i(x\partial_y - y\partial_x)$  is the  $z$ -component of the angular momentum  $\mathbf{L} = \mathbf{x} \times \mathbf{p}$  with

the momentum operator  $\mathbf{P} = -i\nabla = (p_x, p_y, p_z)$ . Two important invariants of the GPE are the mass (or normalization) of the wave function

$$\|\Psi(\mathbf{x}, t)\|^2 := \int_{\mathbb{R}^3} |\Psi(\mathbf{x}, t)|^2 d\mathbf{x} \equiv \int_{\mathbb{R}^3} |\Psi(\mathbf{x}, 0)|^2 d\mathbf{x} = 1, t \geq 0, \quad (2)$$

and the energy per particle

$$E(\Psi(\mathbf{x}, t)) := \int_{\mathbb{R}^3} \left[ \frac{1}{2} |\nabla\Psi|^2 + V(\mathbf{x})|\Psi|^2 + \frac{\beta}{2} |\Psi|^4 + \frac{\lambda}{2} (U_{\text{dip}}(\mathbf{x}) * |\Psi|^2) |\Psi|^2 - \omega R e(\bar{\Psi} L_z \Psi) \right] d\mathbf{x} \equiv E(\Psi(\mathbf{x}, 0)), t \geq 0. \quad (3)$$

Using the equality [13]

$$U_{\text{dip}}(\mathbf{x}) = \frac{3}{4\pi} \frac{1 - 3(\mathbf{x} \cdot \mathbf{n})^2 / |\mathbf{x}|^2}{|\mathbf{x}|^3} = -\delta(\mathbf{x}) - 3\partial_{\mathbf{nn}} \left( \frac{1}{4\pi|\mathbf{x}|} \right), \quad (4)$$

where  $\delta(\mathbf{x})$  is the Dirac distribution function,  $\partial_{\mathbf{n}} = \mathbf{n} \cdot \nabla$ , and  $\partial_{\mathbf{nn}} = \partial_{\mathbf{n}}(\partial_{\mathbf{n}})$ , we can decouple the convolution  $U_{\text{dip}}(\mathbf{x}) * |\Psi|^2$  into two terms

$$U_{\text{dip}}(\mathbf{x}) * |\Psi(\mathbf{x}, t)|^2 = -|\Psi(\mathbf{x}, t)|^2 - 3\partial_{\mathbf{nn}}\varphi(\mathbf{x}, t), \quad (5)$$

where the function  $\varphi$  is defined by

$$\varphi(\mathbf{x}, t) := \frac{1}{4\pi|\mathbf{x}|} * |\Psi(\mathbf{x}, t)|^2, \mathbf{x} \in \mathbb{R}^3, t > 0. \quad (6)$$

Substituting (5) into (1) and noticing (6), we can transform the GPE (1) for rotating dipolar BECs into a Gross-Pitaevskii-Poisson or Schrödinger-Poisson (SP) type system of the following form

$$i\partial_t \Psi(\mathbf{x}, t) = \left[ -\frac{1}{2} \Delta + V(\mathbf{x}) + (\beta - \lambda) |\Psi|^2 - 3\lambda \partial_{\mathbf{nn}} \varphi(\mathbf{x}, t) - \omega L_z \right] \Psi(\mathbf{x}, t), \mathbf{x} \in \mathbb{R}^3, t > 0, \quad (7)$$

$$-\Delta \varphi(\mathbf{x}, t) = |\Psi(\mathbf{x}, t)|^2, \lim_{|\mathbf{x}| \rightarrow \infty} \varphi(\mathbf{x}, t) = 0, \quad (8)$$

and then the energy (3) can be rewritten as

$$E(\Psi(\mathbf{x}, t)) = \int_{\mathbb{R}^3} \left[ \frac{1}{2} |\nabla\Psi|^2 + V(\mathbf{x})|\Psi|^2 + \frac{\beta - \lambda}{2} |\Psi|^4 + \frac{3\lambda}{2} |\partial_{\mathbf{n}} \nabla \varphi|^2 - \omega R e(\bar{\Psi} L_z \Psi) \right] d\mathbf{x}. \quad (9)$$

In many physical experiments of dipolar BECs, the condensates are confined by an anisotropic harmonic potential. When we consider  $V(x, y, z) = (1/2)(\gamma_x^2 x^2 + \gamma_y^2 y^2) + (1/2\varepsilon^4) z^2$ , where  $0 < \varepsilon \ll 1$  is a small parameter describing the

strength of confinement in the  $z$ -direction, the condensates shape will typically like a pancake, and the wave function  $\Psi(\mathbf{x}, t)$  can be factorized into [14, 15]

$$\Psi(\mathbf{x}, t) = e^{-it/2\varepsilon^2} \psi(x, y, t) w_\varepsilon(z), \text{ where } w_\varepsilon(z) = \varepsilon^{-1/2} \pi^{-1/4} e^{-z^2/2\varepsilon^2}. \quad (10)$$

Substituting (10) into the 3D SP system (7)–(8) and the normalization constraint (2), we obtain a quasi-two-dimensional (quasi-2D) system of equations

$$i\partial_t \psi(x, y, t) = \left[ -\frac{1}{2} \Delta + V_2(x, y) + \frac{\beta + \lambda(3n_3^2 - 1)}{\sqrt{2\pi\varepsilon}} |\psi|^2 - \frac{3\lambda}{2} (\partial_{\mathbf{n}_\perp \mathbf{n}_\perp} - n_3^2 \Delta) \varphi_2(x, y, t) - \omega L_z \right] \psi(x, y, t), (x, y) \in \mathbb{R}^2, t \geq 0, \quad (11)$$

$$\begin{aligned} \varphi_2(x, y, t) &= U_2(x, y) * |\psi(x, y, t)|^2, U_2(x, y) \\ &= \frac{1}{2\sqrt{2\pi}^{3/2}} \int_{\mathbb{R}} \frac{e^{-s^2/2}}{\sqrt{x^2 + y^2 + \varepsilon^2 s^2}} ds, \end{aligned} \quad (12)$$

with the constraint

$$\|\psi(x, y, t)\|^2 = \int_{\mathbb{R}^2} |\psi(x, y, t)|^2 dx dy = 1, \quad (13)$$

where  $\Delta = \partial_{xx} + \partial_{yy}$ ,  $V_2(x, y) = (1/2)(\gamma_x^2 x^2 + \gamma_y^2 y^2)$ ,  $\mathbf{n}_\perp = (n_1, n_2)$ ,  $\partial_{\mathbf{n}_\perp} = \mathbf{n}_\perp \cdot \nabla_\perp$  with  $\nabla_\perp = (\partial_x, \partial_y)$ , and  $\partial_{\mathbf{n}_\perp \mathbf{n}_\perp} = \partial_{\mathbf{n}_\perp}(\partial_{\mathbf{n}_\perp})$ . To find the stationary states including ground state of a rotating dipolar BEC, we take the ansatz

$$\psi(x, y, t) = e^{-i\mu t} \phi(x, y), t \geq 0, \quad (14)$$

where  $\mu \in \mathbb{R}$  is the chemical potential and  $\phi(x, y)$  is a time-independent complex function. Substituting (14) into (11)–(13), we obtain the following nonlinear eigenvalue problem

$$\begin{aligned} \left[ -\frac{1}{2} \Delta + V_2(x, y) + \frac{\beta + \lambda(3n_3^2 - 1)}{\sqrt{2\pi\varepsilon}} |\phi|^2 - \frac{3\lambda}{2} (\partial_{\mathbf{n}_\perp \mathbf{n}_\perp} - n_3^2 \Delta) \bar{\varphi}_2(x, y) - \omega L_z \right] \phi(x, y) \\ = \mu \phi(x, y), (x, y) \in \mathbb{R}^2, \end{aligned} \quad (15)$$

$$\bar{\varphi}_2(x, y) = U_2(x, y) * |\phi(x, y)|^2, \quad (16)$$

with the constraint

$$\|\phi\|^2 = \int_{\mathbb{R}^2} |\phi(x, y)|^2 dx dy = 1. \quad (17)$$

During the last decade, some significant mathematical theories and numerical methods for the ground state of dipolar BECs have been reported in the literature [13–17]. Bao et al. [13] transformed the 3D GPE for dipolar BECs into a Gross-Pitaevskii-Poisson system and then proved rigorously

the existence and uniqueness of its ground state. Using dimension reduction, Cai et al. [14] derived two mean-field equations for quasi-1D and quasi-2D dipolar BECs, respectively, and compared their ground state solutions with those of the 3D GPE. The existence and uniqueness of the ground state solutions of these two mean-field equations were established in [15]. In addition, to compute the ground state of dipolar BECs, various efficient numerical methods have been proposed, such as the backward Euler sine pseudospectral method [13], two-level continuation scheme [16], and normalized gradient flow method with nonuniform fast Fourier transform [17]. However, there were only few studies, e.g., [18], concerning the efficient numerical method for computing the ground state of rotating dipolar BECs. In this paper, we will focus on this issue. First, we modify the two-level continuation scheme [16] for 3D dipolar BECs to develop a single-parameter continuation method for quasi-2D rotating dipolar BECs. Next, by treating the chemical potential and the parameter corresponding to the strength of the dipolar interaction as the continuation parameters simultaneously, we propose an efficient two-parameter continuation method, which can trace the ground state solutions of quasi-2D rotating dipolar BECs with increasing the strength of the dipolar interaction. Thus, the

change of the ground-state vortex structure with respect to the dipolar interaction can be easily obtained.

This paper is organized as follows. In Section 2, we briefly describe the spectral collocation method (SCM) for quasi-2D rotating dipolar BECs. In Section 3, we propose single- and two-parameter continuation algorithms for computing the ground state solution of rotating dipolar BECs. In Section 4, we study linear stability analysis for (11). The numerical results are reported in Section 5. Finally, some concluding remarks are given in Section 6.

## 2. A SCM for Quasi-2D Rotating Dipolar BECs

In this section, we describe the SCM using the sine functions as the basis functions for equations (15)–(17). First, since the wave function  $\phi(x, y) \rightarrow 0$  rapidly as  $|(x, y)| \rightarrow \infty$ , we replace the whole space  $\mathbb{R}^2$  in (15) by a sufficiently large domain  $\Omega = (-\ell, \ell)^2$  and impose the zero Dirichlet boundary condition on the function  $\phi(x, y)$ . Next, since  $\phi(x, y)$  is a complex function, we let  $\phi(x, y) = u(x, y) + iv(x, y)$ , where  $u(x, y)$  and  $v(x, y)$  are two real-valued functions. Then, equations (15)–(17) can be rewritten as

$$\begin{aligned} -\frac{1}{2}\Delta u + V_2(x, y)u + \frac{\beta + \lambda(3n_3^2 - 1)}{\sqrt{2\pi\epsilon}}(u^2 + v^2)u - \frac{3\lambda}{2}(\partial_{\mathbf{n}_1\mathbf{n}_1} - n_3^2\Delta)\tilde{\varphi}_2(x, y)u - \omega(xv_y - yv_x) &= \mu u \\ &\text{in } \Omega, \\ -\frac{1}{2}\Delta v + V_2(x, y)v + \frac{\beta + \lambda(3n_3^2 - 1)}{\sqrt{2\pi\epsilon}}(u^2 + v^2)v - \frac{3\lambda}{2}(\partial_{\mathbf{n}_1\mathbf{n}_1} - n_3^2\Delta)\tilde{\varphi}_2(x, y)v + \omega(xu_y - yu_x) &= \mu v \end{aligned} \quad (18)$$

$$u(x, y) = v(x, y) = 0 \text{ on } \partial\Omega,$$

$$\tilde{\varphi}_2(x, y) = U_2(x, y) * (u^2 + v^2), \quad (19)$$

$$\text{constraint : } \int_{\Omega} (u^2 + v^2) dx dy = 1, \quad (20)$$

where  $u_x, v_x$  and  $u_y, v_y$  denote the partial derivatives of  $u$  and  $v$  with respect to  $x$  and  $y$ , respectively. Let  $W_N = \text{span}\{s_j(x)s_k(y) : j, k = 1, 2, \dots, N-1\}$  be the trial function space, where  $s_n(x) = \sin(n\pi(x + \ell)/2\ell)$ . Then,  $\dim W_N = (N-1)^2$  and all the functions of  $W_N$  satisfy the boundary conditions of (18). We choose uniform grids  $\{(x_n, y_m) = (-\ell + n2\ell/N, -\ell + m2\ell/N) : n, m = 1, 2, \dots, N-1\}$  as the collocation points. The SCM for solving (18) is to find  $u_N(x, y) = \sum_{j,k=1}^{N-1} \xi_{jk} s_j(x) s_k(y) \in W_N$  and  $v_N(x, y) = \sum_{j,k=1}^{N-1} \eta_{jk} s_j(x) s_k(y) \in W_N$  such that the residuals vanish at the collocation points, that is,

$$\begin{aligned} -\frac{1}{2}\Delta u_N(x_n, y_m) + V_2(x_n, y_m)u_N(x_n, y_m) \\ + \frac{\beta + \lambda(3n_3^2 - 1)}{\sqrt{2\pi\epsilon}} [u_N^2(x_n, y_m) + v_N^2(x_n, y_m)] u_N(x_n, y_m) \end{aligned}$$

$$\begin{aligned} -\frac{3\lambda}{2}(\partial_{\mathbf{n}_1\mathbf{n}_1} - n_3^2\Delta)\tilde{\varphi}_2(x_n, y_m)u_N(x_n, y_m) \\ - \omega [x_n(v_N)_y(x_n, y_m) - y_m(v_N)_x(x_n, y_m)] \\ - \mu u_N(x_n, y_m) = 0, \quad n, m = 1, 2, \dots, N-1, \end{aligned}$$

$$\begin{aligned} -\frac{1}{2}\Delta v_N(x_n, y_m) + V_2(x_n, y_m)v_N(x_n, y_m) \\ + \frac{\beta + \lambda(3n_3^2 - 1)}{\sqrt{2\pi\epsilon}} [u_N^2(x_n, y_m) + v_N^2(x_n, y_m)] v_N(x_n, y_m) \\ -\frac{3\lambda}{2}(\partial_{\mathbf{n}_1\mathbf{n}_1} - n_3^2\Delta)\tilde{\varphi}_2(x_n, y_m)v_N(x_n, y_m) \\ + \omega [x_n(u_N)_y(x_n, y_m) - y_m(u_N)_x(x_n, y_m)] \\ - \mu v_N(x_n, y_m) = 0, \quad n, m = 1, 2, \dots, N-1. \end{aligned} \quad (21)$$

Denote  $s_{ij} = s_j(x_i)$ ,  $s'_{ij} = s'_j(x_i)$ ,  $s''_{ij} = s''_j(x_i)$ ,  $(v_2)_{nm} = V_2(x_n, y_m)$ ,  $q_{nm} = (\partial_{\mathbf{n}_i \mathbf{n}_j} - n_3^2 \Delta) \tilde{\varphi}_2(x_n, y_m)$ , and define the  $(N-1) \times (N-1)$  matrices

$$\begin{aligned} \mathbf{S} &= [s_{ij}]_{1 \leq i, j \leq N-1}, \mathbf{S}' = [s'_{ij}]_{1 \leq i, j \leq N-1}, \mathbf{S}'' = [s''_{ij}]_{1 \leq i, j \leq N-1}, \\ \mathbf{V}_2 &= [(v_2)_{nm}]_{1 \leq n, m \leq N-1}, \mathbf{Q} = [q_{nm}]_{1 \leq n, m \leq N-1}, \\ \mathbf{U} &= [\xi_{jk}]_{1 \leq j, k \leq N-1}, \mathbf{V} = [\eta_{jk}]_{1 \leq j, k \leq N-1}. \end{aligned} \quad (22)$$

Let the vectors  $\mathbf{u} = \text{vec}(\mathbf{U})$ ,  $\mathbf{v} = \text{vec}(\mathbf{V})$ ,  $\mathbf{v}_2 = \text{vec}(\mathbf{V}_2)$ , and  $\mathbf{q} = \text{vec}(\mathbf{Q})$ , where  $\text{vec}(\mathbf{W})$  denotes the vectorization of a matrix  $\mathbf{W}$  formed by stacking the columns of  $\mathbf{W}$  into a single column vector. Then,  $\mathbf{u}, \mathbf{v}, \mathbf{v}_2, \mathbf{q} \in \mathbb{R}^{(N-1)^2}$  and (21) can be expressed as a nonlinear system of equations involving parameter  $\mu$ :

$$\begin{aligned} H_1(\mathbf{u}, \mathbf{v}, \mu) &= -\frac{1}{2} \mathbf{A} \mathbf{u} + \mathbf{v}_2 \circ (\mathbf{B} \mathbf{u}) + \frac{\beta + \lambda(3n_3^2 - 1)}{\sqrt{2\pi\epsilon}} [(\mathbf{B} \mathbf{u})^2 + (\mathbf{B} \mathbf{v})^2] \circ (\mathbf{B} \mathbf{u}) \\ &\quad - \frac{3\lambda}{2} \mathbf{q} \circ (\mathbf{B} \mathbf{u}) - \omega \mathbf{C} \mathbf{v} - \mu \mathbf{B} \mathbf{u} = \mathbf{0}, \end{aligned} \quad (23)$$

$$\begin{aligned} H_2(\mathbf{u}, \mathbf{v}, \mu) &= -\frac{1}{2} \mathbf{A} \mathbf{v} + \mathbf{v}_2 \circ (\mathbf{B} \mathbf{v}) + \frac{\beta + \lambda(3n_3^2 - 1)}{\sqrt{2\pi\epsilon}} [(\mathbf{B} \mathbf{u})^2 + (\mathbf{B} \mathbf{v})^2] \circ (\mathbf{B} \mathbf{v}) \\ &\quad - \frac{3\lambda}{2} \mathbf{q} \circ (\mathbf{B} \mathbf{v}) + \omega \mathbf{C} \mathbf{u} - \mu \mathbf{B} \mathbf{v} = \mathbf{0}, \end{aligned} \quad (24)$$

where “ $\circ$ ” denotes the Hadamard product,  $\mathbf{w}^k = \mathbf{w} \circ \dots \circ \mathbf{w}$  stands for the  $k$ -times Hadamard products of  $\mathbf{w}$ , and  $\mathbf{A}, \mathbf{B}, \mathbf{C} \in \mathbb{R}^{(N-1)^2 \times (N-1)^2}$  are defined by

$$\begin{aligned} \mathbf{A} &= \mathbf{S} \otimes \mathbf{S}'' + \mathbf{S}'' \otimes \mathbf{S}, \\ \mathbf{B} &= \mathbf{S} \otimes \mathbf{S}, \\ \mathbf{C} &= \mathbf{S}' \otimes (\text{diag}(x_1, \dots, x_{N-1}) \mathbf{S}) - (\text{diag}(y_1, \dots, y_{N-1}) \mathbf{S}) \otimes \mathbf{S}', \end{aligned} \quad (25)$$

where “ $\otimes$ ” denotes the Kronecker product and  $\text{diag}(d_1, \dots, d_{N-1})$  is an  $(N-1) \times (N-1)$  diagonal matrix with  $d_1, \dots, d_{N-1}$  as the diagonal entries. Moreover, the constraint condition (20) can be expressed as

$$\ell^2 (\mathbf{u}^T \mathbf{u} + \mathbf{v}^T \mathbf{v}) = 1. \quad (26)$$

To compute the matrix  $\mathbf{Q}$ , we need to efficiently discretize the convolution  $\tilde{\varphi}_2$ . Based on the convolution theory, it is natural to consider using the Fourier transform to compute it. To be precise, since  $\mathcal{F}[\tilde{\varphi}_2] = \mathcal{F}[U_2 * (u^2 + v^2)] = \mathcal{F}[U_2] \cdot \mathcal{F}[u^2 + v^2]$ , where  $\mathcal{F}$  denotes the 2D Fourier transform operator, we have that

$$\tilde{\varphi}_2 = \mathcal{F}^{-1} [\mathcal{F}[U_2] \cdot \mathcal{F}[u^2 + v^2]], \quad (27)$$

where  $\mathcal{F}^{-1}$  denotes the 2D inverse Fourier transform operator, and the Fourier transform  $\mathcal{F}[U_2]$  of the integral  $U_2$  is given by [14]

$$\mathcal{F}[U_2](k_x, k_y) = \frac{1}{2\pi^2} \int_{\mathbb{R}} \frac{e^{-\epsilon^2 s^2/2}}{k_x^2 + k_y^2 + s^2} ds. \quad (28)$$

Since the integrand in (28) decays exponentially fast, we can replace the domain of integration  $\mathbb{R}$  by a sufficiently large interval  $[-\ell, \ell]$  and then evaluate the definite integral via numerical quadratures, e.g., composite trapezoidal rule or Gaussian quadrature. Moreover, in practical computations, since we only know the values of  $u$  and  $v$  on the grid points of the domain  $\Omega$ , the Fourier transform and the inverse Fourier transform mentioned above are replaced by the discrete Fourier transform and the inverse discrete Fourier transform, respectively, and can be efficiently computed via the fast Fourier transform (FFT) and the inverse fast Fourier transform (IFFT).

In our numerical computations, we incorporate the SCM in the continuation method and use single- or two-parameter continuation algorithms, which are described in the next section, to compute the ground state solution of a quasi-2D rotating dipolar BECs. In the continuation method, we need the Jacobian matrix associated with  $H = [H_1, H_2]^T$ , which is given as

$$DH(\mathbf{u}, \mathbf{v}, \mu) = \begin{bmatrix} D_{\mathbf{u}} H_1(\mathbf{u}, \mathbf{v}, \mu) & D_{\mathbf{v}} H_1(\mathbf{u}, \mathbf{v}, \mu) & D_{\mu} H_1(\mathbf{u}, \mathbf{v}, \mu) \\ D_{\mathbf{u}} H_2(\mathbf{u}, \mathbf{v}, \mu) & D_{\mathbf{v}} H_2(\mathbf{u}, \mathbf{v}, \mu) & D_{\mu} H_2(\mathbf{u}, \mathbf{v}, \mu) \end{bmatrix} \in \mathbb{R}^{2(N-1)^2 \times (2(N-1)^2 + 1)}, \quad (29)$$

where

$$\begin{aligned} D_{\mathbf{u}} H_1(\mathbf{u}, \mathbf{v}, \mu) &= -\frac{1}{2} \mathbf{A} + \text{diag}(\mathbf{v}_2) \mathbf{B} \\ &\quad + \frac{\beta + \lambda(3n_3^2 - 1)}{\sqrt{2\pi\epsilon}} \text{diag}(3(\mathbf{B} \mathbf{u})^2 + (\mathbf{B} \mathbf{v})^2) \mathbf{B} \\ &\quad - \frac{3\lambda}{2} \text{diag}(\mathbf{q}) \mathbf{B} - \mu \mathbf{B}, \end{aligned} \quad (30)$$

$$D_{\mathbf{v}} H_1(\mathbf{u}, \mathbf{v}, \mu) = \frac{\beta + \lambda(3n_3^2 - 1)}{\sqrt{2\pi\epsilon}} \text{diag}(2(\mathbf{B} \mathbf{v}) \circ (\mathbf{B} \mathbf{u})) \mathbf{B} - \omega \mathbf{C}, \quad (31)$$

$$D_{\mu} H_1(\mathbf{u}, \mathbf{v}, \mu) = -\mathbf{B} \mathbf{u}, \quad (32)$$

$$D_{\mathbf{u}} H_2(\mathbf{u}, \mathbf{v}, \mu) = \frac{\beta + \lambda(3n_3^2 - 1)}{\sqrt{2\pi\epsilon}} \text{diag}(2(\mathbf{B} \mathbf{u}) \circ (\mathbf{B} \mathbf{v})) \mathbf{B} + \omega \mathbf{C}, \quad (33)$$

$$\begin{aligned}
D_v H_2(\mathbf{u}, \mathbf{v}, \mu) = & -\frac{1}{2} \mathbf{A} + \text{diag}(\mathbf{v}_2) \mathbf{B} \\
& + \frac{\beta + \lambda(3n_3^2 - 1)}{\sqrt{2\pi\epsilon}} \text{diag}((\mathbf{B}\mathbf{u})^2 + 3(\mathbf{B}\mathbf{v})^2) \mathbf{B} \\
& - \frac{3\lambda}{2} \text{diag}(\mathbf{q}) \mathbf{B} - \mu \mathbf{B},
\end{aligned} \tag{34}$$

$$D_\mu H_2(\mathbf{u}, \mathbf{v}, \mu) = -\mathbf{B}\mathbf{v}, \tag{35}$$

and  $\text{diag}(\mathbf{c})$  is a diagonal matrix with the components of the vector  $\mathbf{c}$  as the diagonal entries.

### 3. Efficient Two-Parameter Continuation Algorithms

Jeng et al. [16] proposed a two-level continuation scheme for computing the ground state solution of a 3D dipolar BEC, which is governed by a stationary state SP system. The two major differences between the system (15)–(17) for a quasi-2D rotating dipolar BEC and the stationary state SP system in [16] are that (i) in the former, the wave function  $\phi$  is a complex-valued function, while in the latter, the wave function is a real-valued function. (ii) The function  $\tilde{\varphi}_2$  in (16) is defined by a convolution, while the corresponding one in the SP system is defined by a Poisson equation. However, the structures of these two systems are similar. We can modify the two-level continuation scheme in [16] to compute the ground state solution of a quasi-2D rotating dipolar BEC which is stated as follows.

First, we rewrite the complex system (15)–(17) into a real system, which is described in (18)–(20). Starting with  $\tilde{\varphi}_2(x, y) = 0$ , (18) is the governing equation for a rotating BEC. By treating the chemical potential  $\mu$  as the continuation parameter, we use an efficient continuation algorithm [19–22] to trace the ground state solution curve of (18) bifurcating at the first bifurcation point. The constraint condition (20) is set as the target point for the curve-tracking. Next, we compute the convolution in (19) to obtain an approximation of  $\tilde{\varphi}_2$  and compute  $(\partial_{\mathbf{n}_1 \mathbf{n}_1} - n_3^2 \Delta) \tilde{\varphi}_2$  for the next step continuation algorithm. Here, the operators  $*$ ,  $\partial_{\mathbf{n}_1 \mathbf{n}_1}$ , and  $\Delta$  can be efficiently computed via the FFT and the IFFT. Then, we use the continuation algorithm again to trace the ground state solution curve of (18) bifurcating at the first bifurcation point until the constraint (20) is satisfied. Similarly, we use the FFT and IFFT again to compute the approximation of  $\tilde{\varphi}_2$  and  $(\partial_{\mathbf{n}_1 \mathbf{n}_1} - n_3^2 \Delta) \tilde{\varphi}_2$  for the next step continuation algorithm. We repeat the same process as above until two consecutive bifurcation points are close enough. Then, instead of tracing the ground state solution curve of (18), we perform the Newton method to solve (18) and (20) simultaneously and then update the approximation of  $\tilde{\varphi}_2$ . We keep repeating the process until the approximation of  $\tilde{\varphi}_2$  converges. Then, the desired ground state solution of (18)–(20) can be obtained. A detailed description of this continuation scheme is as follows.

Note that in Algorithm 1, the purpose of Step 1 is to obtain an appropriate approximate solution as the starting

point for Step 2. And the purpose of Step 2 is to correct the function  $\tilde{\varphi}_2$ . Moreover, in the while loop of Step 1, when  $i = 1$ , we obtain the ground state solution  $\phi_1^* = u_1^* + iv_1^*$  of a rotating BEC and then set  $(\tilde{\varphi}_2)_1 = U_2 * |\phi_1^*|^2$  to continue the next iteration of the while loop. This means that we take  $\phi_1^*$  as an approximate ground state solution of a rotating dipolar BEC and then use the iterative way to get a better approximation. Hence, although the initial choice  $(\tilde{\varphi}_2)_0 = 0$ , we actually use  $(\tilde{\varphi}_2)_1 = U_2 * |\phi_1^*|^2$  as an initial approximation of  $\tilde{\varphi}_2$ . Additionally, if a suitable approximation  $\phi_{\text{app}}$  for the ground state solution of a rotating dipolar BEC can be easily known in advance (e.g., the Thomas-Fermi approximation is a suitable one when  $\beta$  is large), we can choose  $(\tilde{\varphi}_2)_0 = U_2 * |\phi_{\text{app}}|^2$  instead of  $(\tilde{\varphi}_2)_0 = 0$ .

To investigate how the ground-state vortex structures are affected by the strength of the dipolar interaction, we can use Algorithm 1 to compute the ground state solutions for various values of  $\lambda$ . However, this is obviously time-consuming because we must repeatedly implement Algorithm 1. In the following, we will describe a two-parameter continuation algorithm which can effectively show the change of the ground-state vortex structures as  $\lambda$  gradually increases.

Let  $\lambda = \gamma\beta$ . In the first step of the two-parameter continuation algorithm, we fix  $\gamma = \gamma_0$  and implement Algorithm 1 to compute the ground state solution of (18)–(20) with  $\lambda = \gamma_0\beta$ , where the chemical potential  $\mu$  is treated as the continuation parameter. Set this solution as  $(u^{(0)}, v^{(0)}, \mu^{(0)})$ . In the second step, we add  $\gamma$  as the second continuation parameter and continue to compute the ground state solutions for other values of  $\gamma$ . Here, the ground state solution  $\mathbf{y}^{(0)} = (u^{(0)}, v^{(0)}, \mu^{(0)}, \gamma^{(0)} = \gamma_0)$  is used as the starting point. The procedure of tracing next accepted ground state solution  $\mathbf{y}^{(1)} = (u^{(1)}, v^{(1)}, \mu^{(1)}, \gamma^{(1)})$  of (18)–(20) with  $\lambda = \gamma^{(1)}\beta$  consists of two parts:

- (I) Find an approximate ground state solution for the next value of  $\gamma$ :

We fix  $\tilde{\varphi}_2 = \tilde{\varphi}_2^{(0)} := U_2 * ((u^{(0)})^2 + (v^{(0)})^2)$  in (18) and then perform the Euler predictor-Newton corrector process once to obtain a solution of (18) with  $\tilde{\varphi}_2 = \tilde{\varphi}_2^{(0)}$  under the normalization condition (20), where  $\mu$  and  $\gamma$  are treated as the continuation parameters simultaneously.

- (II) Correct  $\tilde{\varphi}_2$  by the iterative way:

We repeatedly update the approximation of  $\tilde{\varphi}_2$  and solve (18) and (20) simultaneously until the approximation of  $\tilde{\varphi}_2$  converges. Then, the ground state solution  $\mathbf{y}^{(1)}$  of (18)–(20) with  $\lambda = \gamma^{(1)}\beta$  is obtained.

Using  $\mathbf{y}^{(1)}$  instead of  $\mathbf{y}^{(0)}$  and repeating (I) and (II), we can obtain the next accepted ground state solution  $\mathbf{y}^{(2)} = (u^{(2)}, v^{(2)}, \mu^{(2)}, \gamma^{(2)})$  of (18)–(20) with  $\lambda = \gamma^{(2)}\beta$ . Similarly, we can continue to trace the ground state solutions  $\mathbf{y}^{(3)}$ ,  $\mathbf{y}^{(4)}$ , and so on, until the desired target value of  $\gamma$  is reached. A detailed description of this two-parameter continuation algorithm is as follows.

Input:

$i :=$  the  $i$ -th iterate of the iterative continuation scheme.

$\tau_1 :=$  accuracy tolerance for two consecutive bifurcation points.

$\tau_2 :=$  accuracy tolerance for  $(\tilde{\varphi}_2)_{i,j}$ .

$(\tilde{\varphi}_2)_0 := 0, i := 0$ .

Step 1. Compute the first bifurcation point  $(0, 0, \mu_1)$  of (18) with  $\tilde{\varphi}_2 = (\tilde{\varphi}_2)_0$ .

**while** ( $i = 0$  or  $|\mu_i - \mu_{i+1}| > \tau_1$ ) **do**

(i)  $i = i + 1$ .

(ii) Treat  $\mu$  as the continuation parameter and use the classical continuation algorithm to trace the ground state solution curve of (18) with  $\tilde{\varphi}_2 = (\tilde{\varphi}_2)_{i-1}$  until the constraint (20) is satisfied. Set this solution as  $(u_i^*, v_i^*, \mu_i^*)$ .

(iii) Compute  $(\tilde{\varphi}_2)_i = U_2 * ((u_i^*)^2 + (v_i^*)^2)$  and  $(\partial_{\mathbf{n}_\perp \mathbf{n}_\perp} - n_3^2 \Delta)(\tilde{\varphi}_2)_i$ .

(iv) Compute the first bifurcation point  $(0, 0, \mu_{i+1})$  of (18) with  $\tilde{\varphi}_2 = (\tilde{\varphi}_2)_i$ .

**end**

Step 2. Set  $j = 0$  and  $(u_{i,0}^*, v_{i,0}^*, \mu_{i,0}^*) = (u_i^*, v_i^*, \mu_i^*)$ ,  $(\tilde{\varphi}_2)_{i,0} = (\tilde{\varphi}_2)_i$ .

**while** ( $j = 0$  or  $\|(\tilde{\varphi}_2)_{i,j} - (\tilde{\varphi}_2)_{i,j-1}\|_\infty > \tau_2$ ) **do**

(i)  $j = j + 1$ .

(ii) Use the approximate solution  $(u_{i,j-1}^*, v_{i,j-1}^*, \mu_{i,j-1}^*)$  as the initial guess, and perform the Newton method to solve (18) with  $\tilde{\varphi}_2 = (\tilde{\varphi}_2)_{i,j-1}$  and (20) simultaneously.

(iii) Set the approximate solution obtained in (ii) by  $(u_{i,j}^*, v_{i,j}^*, \mu_{i,j}^*)$ .

(iv) Compute  $(\tilde{\varphi}_2)_{i,j} = U_2 * ((u_{i,j}^*)^2 + (v_{i,j}^*)^2)$  and  $(\partial_{\mathbf{n}_\perp \mathbf{n}_\perp} - n_3^2 \Delta)(\tilde{\varphi}_2)_{i,j}$ .

**end**

The desired ground state solution  $(u^*, v^*, \mu^*) = (u_{i,j}^*, v_{i,j}^*, \mu_{i,j}^*)$ .

ALGORITHM 1: A single-parameter continuation algorithm for computing the ground state of a quasi-2D rotating dipolar BEC.

Input:

$\gamma_0 :=$  the initial value of the parameter  $\gamma$ .

$\gamma_{end} :=$  the final value of the parameter  $\gamma$ .

$\tau :=$  accuracy tolerance for  $(\tilde{\varphi}_2^{(i)})_j$ .

Step 1. Use Algorithm 1 to compute the ground state solution of (18)–(20) with  $\lambda = \gamma_0 \beta$ . Set this solution as  $(u^{(0)}, v^{(0)}, \mu^{(0)})$ .

Step 2. Add  $\gamma$  as the second continuation parameter and trace the ground state solution curve of (18)–(20) until  $\gamma \geq \gamma_{end}$ :

Use  $(u^{(0)}, v^{(0)}, \mu^{(0)}, \gamma^{(0)}) = (u^{(0)}, v^{(0)}, \mu^{(0)}, \gamma_0)$  as the starting point and set  $i = 0$ .

**while**  $\gamma^{(i)} < \gamma_{end}$  **do**

(i)  $i = i + 1$ .

(ii) Compute  $\tilde{\varphi}_2^{(i-1)} = U_2 * ((u^{(i-1)})^2 + (v^{(i-1)})^2)$  and  $(\partial_{\mathbf{n}_\perp \mathbf{n}_\perp} - n_3^2 \Delta)\tilde{\varphi}_2^{(i-1)}$ .

(iii) Treat  $\mu$  and  $\gamma$  as the continuation parameters simultaneously, and perform the predictor-corrector process once to obtain a solution of (18) with  $\tilde{\varphi}_2 = \tilde{\varphi}_2^{(i-1)}$  under the normalization condition (20). Set this solution as  $(u^{(i,0)}, v^{(i,0)}, \mu^{(i,0)}, \gamma^{(i,0)})$ .

(iv) Set  $j = 0$  and compute  $\tilde{\varphi}_2^{(i,0)} = U_2 * ((u^{(i,0)})^2 + (v^{(i,0)})^2)$ ,  $(\partial_{\mathbf{n}_\perp \mathbf{n}_\perp} - n_3^2 \Delta)\tilde{\varphi}_2^{(i,0)}$ .

(v)  $j = j + 1$ .

(vi) Use  $(u^{(i,j-1)}, v^{(i,j-1)}, \mu^{(i,j-1)}, \gamma^{(i,j-1)})$  as the initial guess and perform Newton's method to solve (18) with  $\tilde{\varphi}_2 = \tilde{\varphi}_2^{(i,j-1)}$  and (20) simultaneously. Set this solution as  $(u^{(i,j)}, v^{(i,j)}, \mu^{(i,j)}, \gamma^{(i,j)})$ .

(vii) Compute  $\tilde{\varphi}_2^{(i,j)} = U_2 * ((u^{(i,j)})^2 + (v^{(i,j)})^2)$  and  $(\partial_{\mathbf{n}_\perp \mathbf{n}_\perp} - n_3^2 \Delta)\tilde{\varphi}_2^{(i,j)}$ .

(viii) Repeat the procedure (v)–(vii) until  $\|\tilde{\varphi}_2^{(i,j)} - \tilde{\varphi}_2^{(i,j-1)}\|_\infty < \tau$ , then set  $(u^{(i)}, v^{(i)}, \mu^{(i)}, \gamma^{(i)}) = (u^{(i,j)}, v^{(i,j)}, \mu^{(i,j)}, \gamma^{(i,j)})$  which is the ground state solution of (18)–(20) with  $\lambda = \gamma^{(i)} \beta$ .

**end**

ALGORITHM 2: A two-parameter continuation algorithm for computing the ground state of a quasi-2D rotating dipolar BEC.

Note that in practical computations, we suggest choosing  $\gamma_0 = 0$ , which means that the dipolar interaction is absent, and then (18)–(20) are simplified to the system of equations for rotating BECs. Some efficient continuation algorithms

[19–21] have been proposed for computing the ground state solution of rotating BECs. We can use one of these algorithms instead of Algorithm 1 in Step 1. In addition, Step 2 has the advantage that it can trace the ground state solutions

TABLE 1: The first bifurcation points and associated energy levels of (15) with  $V_2(x, y) = (1.003x^2 + 0.997y^2)/2$ ,  $\varepsilon = 1/\sqrt{5}$ ,  $\mathbf{n} = (1, 0, 1)/\sqrt{2}$ ,  $\beta = 500$ ,  $\lambda = 200$ , and  $\omega = 0.9$ .

$i$	Step 1 of Algorithm 1			$j$	Step 2 of Algorithm 1	
	$\mu_i$	$ \mu_i - \mu_{i-1} $	$\mu_i^*$		$\mu_{2,j}^*$	$\ (\tilde{\varphi}_2)_{2,j} - (\tilde{\varphi}_2)_{2,j-1}\ _\infty$
1	0.999994079	—	6.948810421	1	6.809820932	3.05e-04
2	0.813189699	0.186804379	6.835483577	2	6.810717813	4.63e-05
3	0.800819436	0.012370264	—	3	6.810229110	4.02e-05
				4	6.809399974	3.87e-05
				5	6.808222809	3.97e-05
				6	6.806631955	4.82e-05
				7	6.804621207	5.55e-05
				8	6.802425277	5.53e-05
				9	6.800456124	4.69e-05
				10	6.798965356	3.57e-05
				11	6.797954351	2.64e-05
				12	6.797308616	1.95e-05
				13	6.796906662	1.40e-05
				14	6.796657470	9.84e-06
				15	6.796501681	6.89e-06
				16	6.796402891	4.80e-06
				17	6.796339258	3.33e-06
				18	6.796297675	2.30e-06
				19	6.796270168	1.58e-06
				20	6.796251800	1.09e-06
				21	6.796239445	7.44e-07
					$\mu^* = 6.796239445$	
Total execution time: 723.39 sec						

with increasing the value of  $\gamma$ . Thus, the evolution of the ground-state vortex structure with respect to the dipolar interaction can be easily observed.

#### 4. Linear Stability Analysis

The aim of this section is to study linear stability analysis for (11). We impose an infinitesimal perturbation  $r(x, y, t)$  on the wave function  $\psi(x, y, t)$  in (14) by letting

$$\psi(x, y, t) = e^{-i\mu t} (\phi(x, y) + r(x, y, t)), \quad (36)$$

where  $(\mu, \phi(x, y))$  is the solution of (15) and  $r(x, y, t)$  is a complex function. Substituting (36) into (11) and using the approximation  $\varphi_2 = U_2 * |\psi|^2 \approx U_2 * |\phi|^2 = \tilde{\varphi}_2$ , we obtain

$$e^{-i\mu t} \left[ \mu(\phi + r) + i \frac{\partial r}{\partial t} \right] \approx e^{-i\mu t} \left[ -\frac{1}{2} \Delta + V_2 + \frac{\beta + \lambda(3n_3^2 - 1)}{\sqrt{2\pi\varepsilon}} (|\phi|^2 + \phi\bar{r} + \bar{\phi}r + |r|^2) - \frac{3\lambda}{2} (\partial_{n_1 n_1} - n_3^2 \Delta) \tilde{\varphi}_2 - \omega L_z \right] (\phi + r), \quad (37)$$

$$\begin{aligned} \Rightarrow i \frac{\partial r}{\partial t} \approx & \left[ -\frac{1}{2} \Delta + V_2 + \frac{\beta + \lambda(3n_3^2 - 1)}{\sqrt{2\pi\varepsilon}} |\phi|^2 - \frac{3\lambda}{2} (\partial_{n_1 n_1} - n_3^2 \Delta) \tilde{\varphi}_2 - \omega L_z - \mu \right] \phi \\ & + \left[ -\frac{1}{2} \Delta + V_2 - \frac{3\lambda}{2} (\partial_{n_1 n_1} - n_3^2 \Delta) \tilde{\varphi}_2 - \omega L_z - \mu \right] r \\ & + \frac{\beta + \lambda(3n_3^2 - 1)}{\sqrt{2\pi\varepsilon}} (2|\phi|^2 r + \phi^2 \bar{r} + 2\phi |r|^2 + \bar{\phi} r^2 + |r|^2 r). \end{aligned} \quad (38)$$

Then taking (15) into account and linearizing (i.e., neglecting terms of  $O(r^k)$  and  $k \geq 2$ ), we obtain the following linearized equation which models the development of the perturbation  $r(x, y, t)$ :

$$i \frac{\partial r}{\partial t} = \left[ -\frac{1}{2} \Delta + V_2(x, y) - \frac{3\lambda}{2} (\partial_{n_1 n_1} - n_3^2 \Delta) \tilde{\varphi}_2(x, y) - \omega L_z - \mu \right] r + \frac{\beta + \lambda(3n_3^2 - 1)}{\sqrt{2\pi\varepsilon}} (2|\phi|^2 r + \phi^2 \bar{r}). \quad (39)$$

Since (39) includes both  $r$  and  $\bar{r}$ , we use the technique described in [23–25] to decompose the perturbation  $r(x, y, t)$  as

$$r(x, y, t) = p(x, y) e^{at} + \overline{q(x, y)} e^{\bar{a}t}, \quad (40)$$

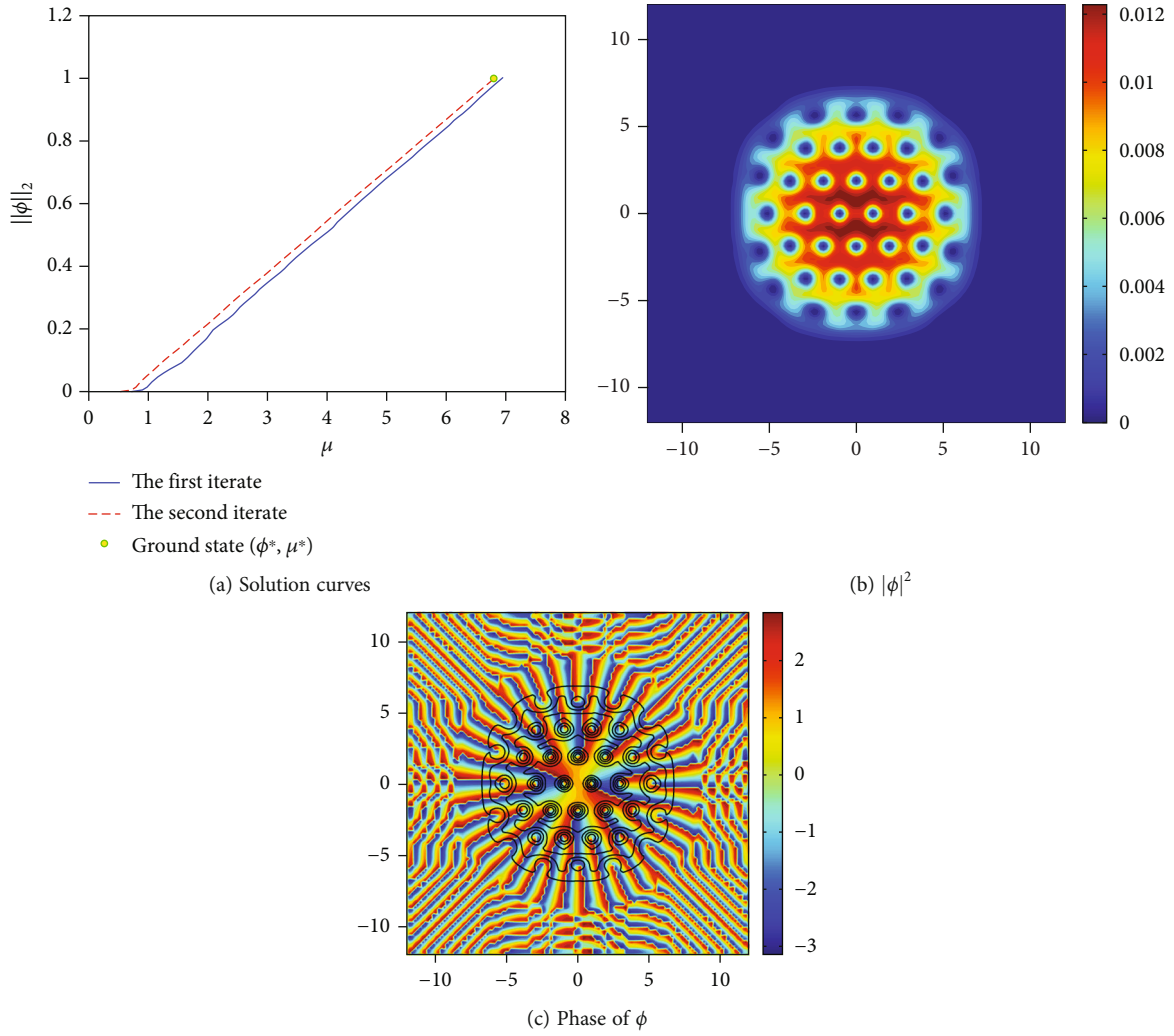


FIGURE 1: The solution curves, the contour plot of  $|\phi|^2$ , and the phase of  $\phi$  for the ground state solution of (15), where  $V_2(x, y) = (1.003x^2 + 0.997y^2)/2$ ,  $\varepsilon = 1/\sqrt{5}$ ,  $\mathbf{n} = (1,0,1)/\sqrt{2}$ ,  $\beta = 500$ ,  $\lambda = 200$ , and  $\omega = 0.9$ .

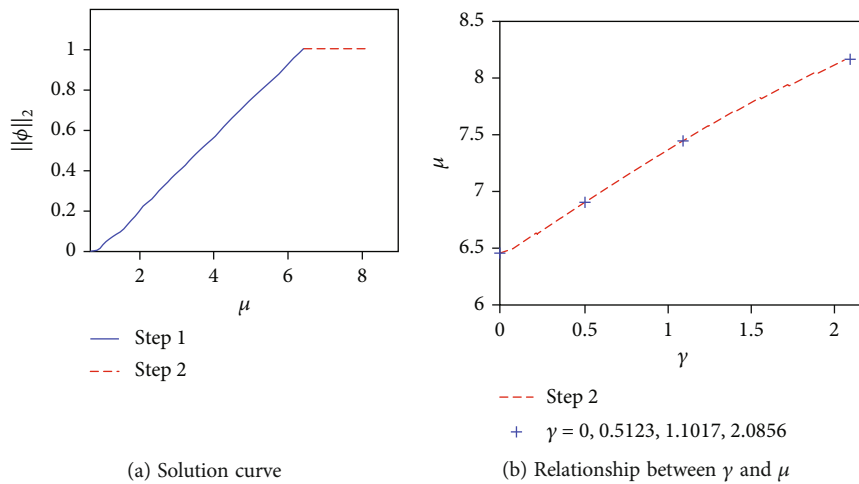


FIGURE 2: Implementing Algorithm 2 for the ground state solution branch of (15), where  $V_2(x, y) = (1.003x^2 + 0.997y^2)/2$ ,  $\varepsilon = 1/\sqrt{5}$ ,  $\mathbf{n} = (1,0,1)/\sqrt{2}$ ,  $\omega = 0.9$ ,  $\beta = 500$ , and  $\lambda = \gamma\beta$ .

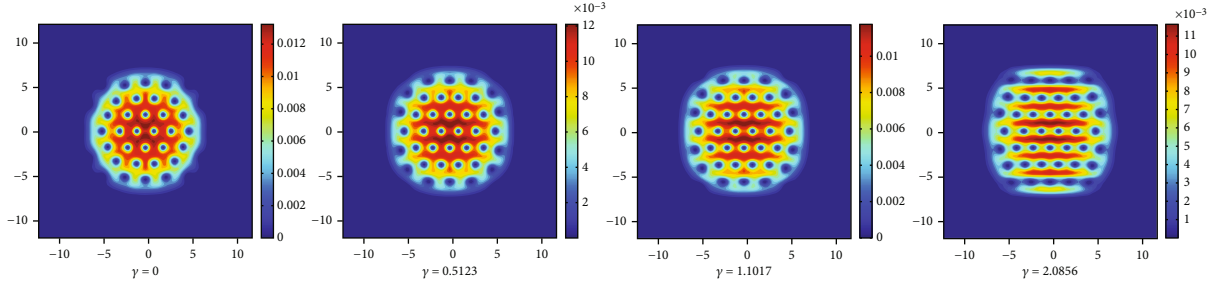


FIGURE 3: The contours of the ground state density function  $|\phi|^2$  of (15), where  $V_2(x, y) = (1.003x^2 + 0.997y^2)/2$ ,  $\varepsilon = 1/\sqrt{5}$ ,  $\mathbf{n} = (1, 0, 1)/\sqrt{2}$ ,  $\omega = 0.9$ ,  $\beta = 500$ , and  $\lambda = \gamma\beta$ .

TABLE 2: The execution time (in seconds) for computing the ground state solution of Example 2 by implementing Algorithm 2. NIW: number of iterations in the while loop of Step 2.

	$\gamma$	NIW	Time (s)
Step 1	0	—	349.10
Step 2	0–0.5123	4	158.57
	0.5123–1.1017	4	85.51
	1.1017–2.0856	6	307.20
Total time of Step 2: 551.28			
Total		14	900.38

where  $p(x, y)$  and  $q(x, y)$  are complex functions, and  $\alpha \in \mathbb{C}$  is the unknown coefficient yet to be determined. Inserting (40) into (39), we obtain a linear eigenvalue problem of the form

$$\begin{aligned} & \left[ -\frac{1}{2}\Delta + V_2(x, y) + 2\frac{\beta + \lambda(3n_3^2 - 1)}{\sqrt{2\pi\varepsilon}}|\phi|^2 - \frac{3\lambda}{2}(\partial_{\mathbf{n}_1\mathbf{n}_1} - n_3^2\Delta)\tilde{\varphi}_2(x, y) - \omega L_z - \mu \right] p(x, y) \\ & + \frac{\beta + \lambda(3n_3^2 - 1)}{\sqrt{2\pi\varepsilon}}\phi^2 q(x, y) = i\alpha p(x, y), \end{aligned} \quad (41)$$

$$\begin{aligned} & \left[ -\frac{1}{2}\Delta + V_2(x, y) + 2\frac{\beta + \lambda(3n_3^2 - 1)}{\sqrt{2\pi\varepsilon}}|\phi|^2 - \frac{3\lambda}{2}(\partial_{\mathbf{n}_1\mathbf{n}_1} - n_3^2\Delta)\tilde{\varphi}_2(x, y) - \omega L_z - \mu \right] q(x, y) \\ & + \frac{\beta + \lambda(3n_3^2 - 1)}{\sqrt{2\pi\varepsilon}}\overline{\phi^2} p(x, y) = -i\alpha q(x, y). \end{aligned} \quad (42)$$

Let  $A(\phi) = \begin{bmatrix} f_{11}(\phi) & f_{12}(\phi) \\ f_{12}(\phi) & f_{22}(\phi) \end{bmatrix}$  be an operator matrix with

$$\begin{aligned} f_{11}(\phi) &= -\frac{1}{2}\Delta + V_2(x, y) + 2\frac{\beta + \lambda(3n_3^2 - 1)}{\sqrt{2\pi\varepsilon}}|\phi|^2 \\ & - \frac{3\lambda}{2}(\partial_{\mathbf{n}_1\mathbf{n}_1} - n_3^2\Delta)\tilde{\varphi}_2(x, y) - \omega L_z - \mu, \end{aligned} \quad (43)$$

$$f_{12}(\phi) = \frac{\beta + \lambda(3n_3^2 - 1)}{\sqrt{2\pi\varepsilon}}\phi^2, \quad (44)$$

and  $B = \text{diag}(i, -i) \in \mathbb{C}^{2 \times 2}$ ,  $\mathbf{r} = [p(x, y), q(x, y)]^T$ . Then, (41)

and (42) can be written in matrix form as

$$A(\phi)\mathbf{r} = \alpha B\mathbf{r}. \quad (45)$$

This eigenvalue problem has the following property.

**Proposition 1.** *The complex eigenvalues of (45) must come in conjugate pairs as  $\{\alpha, \bar{\alpha}\}$ .*

*Proof.* Let  $\alpha, \mathbf{r}$  be a complex eigenvalue-eigenvector pair of (45). From (45), we have

$$\overline{A(\phi)}\overline{\mathbf{r}} = \bar{\alpha}\overline{B}\overline{\mathbf{r}}. \quad (46)$$

Take  $Q = \begin{bmatrix} 0 & 1 \\ 1 & 0 \end{bmatrix}$ . Then,  $Q^{-1} = Q$ ,  $QA(\phi)Q^{-1} = \overline{A(\phi)}$ ,  $QBQ^{-1} = \overline{B}$ , and from (46), we have

$$A(\phi)Q^{-1}\overline{\mathbf{r}} = \bar{\alpha}BQ^{-1}\overline{\mathbf{r}}, \quad (47)$$

which means that  $\bar{\alpha}, Q^{-1}\overline{\mathbf{r}}$  is a complex eigenvalue-eigenvector pair of (45). Therefore, the complex eigenvalues of (45) always appear in conjugate pairs  $\{\alpha, \bar{\alpha}\}$ .  $\square$

When all eigenvalues  $\alpha$  of (45) have negative or zero real parts; then, the corresponding perturbation  $r(x, y, t)$  in (40) decays exponentially or is bounded; hence, the wave function is linearly stable. In contrast, if at least one eigenvalue has a positive real part; then,  $r(x, y, t)$  grows exponentially; hence, the wave function is linearly unstable. Unfortunately, since (45) includes the unknown wave function  $\phi$ , it is difficult to analyze the sign of the real part of its eigenvalues

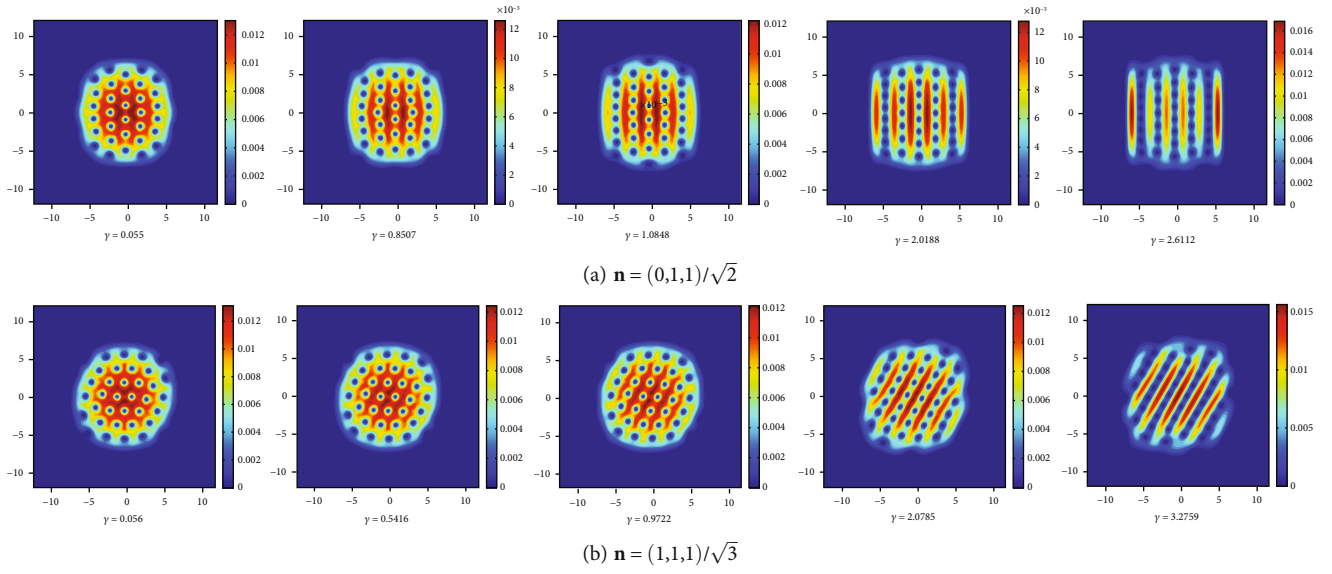


FIGURE 4: The contours of the ground state density function  $|\phi|^2$  of (15), where  $V_2(x, y) = (1.003x^2 + 0.997y^2)/2$ ,  $\varepsilon = 1/\sqrt{5}$ ,  $\omega = 0.9$ ,  $\beta = 500$ , and  $\lambda = \gamma\beta$ .

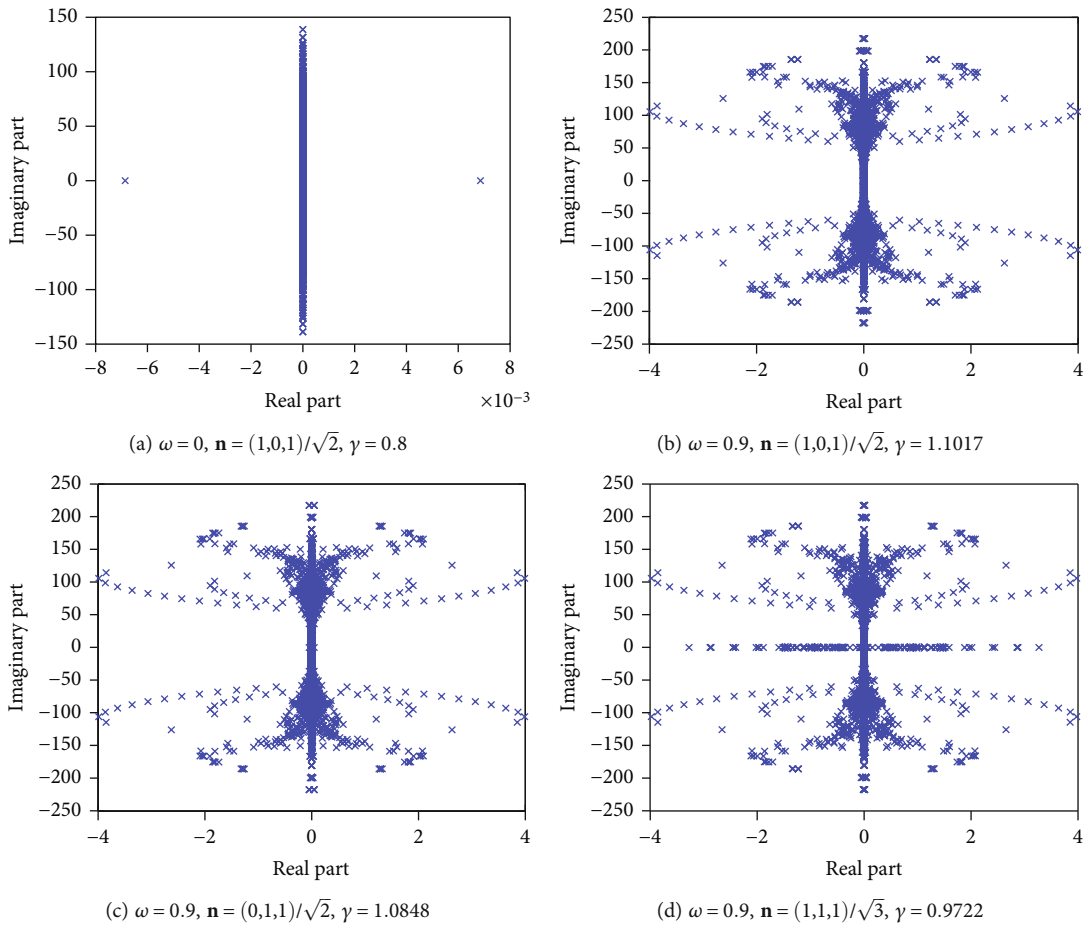


FIGURE 5: The discrete eigenvalues distribution of (45) for quasi-2D (rotating) dipolar BEC, where  $V_2(x, y) = (1.003x^2 + 0.997y^2)/2$ ,  $\varepsilon = 1/\sqrt{5}$ ,  $\beta = 500$ , and  $\lambda = \gamma\beta$ .

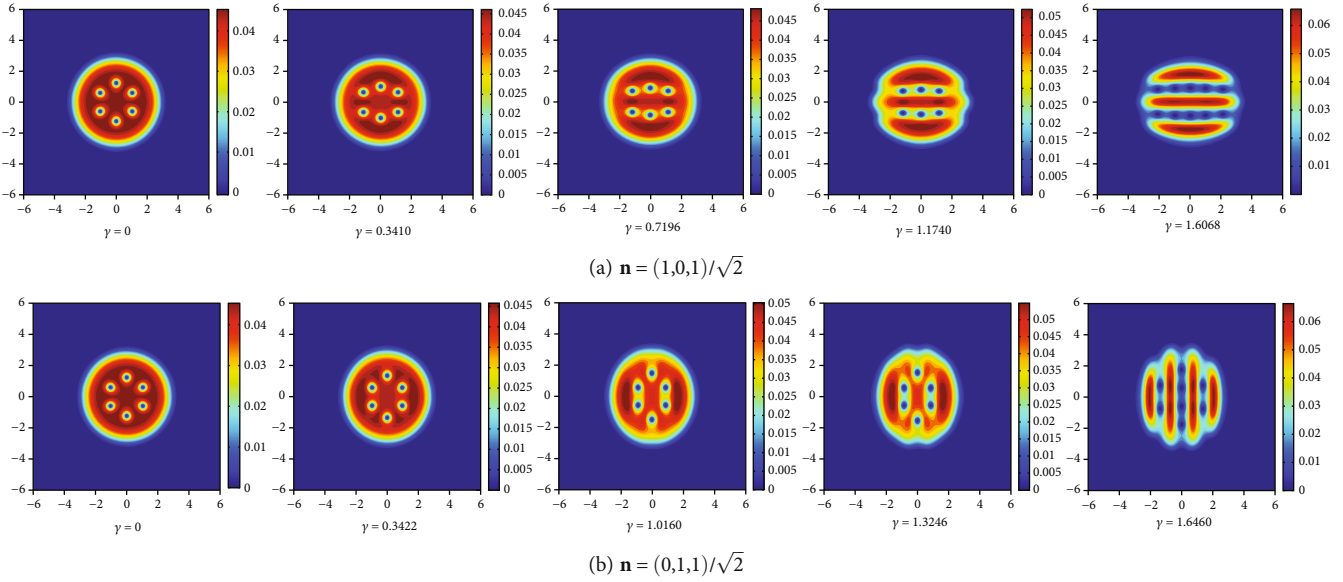


FIGURE 6: The contours of the ground state density function  $|\phi|^2$  of (15), where  $V_2(x, y) = (1.003x^2 + 0.997y^2)/2 + (1.003x^2 + 0.997y^2)^2/4$ ,  $\varepsilon = 1/\sqrt{5}$ ,  $\omega = 1.7$ ,  $\beta = 500$ , and  $\lambda = \gamma\beta$ .

TABLE 3: The execution time (in seconds) for computing the ground state solution of Example 5(2) by implementing Algorithm 2. NIW: number of iterations in the while loop of Step 2.

	$\gamma$	NIW	Time (s)	
Step 1	0	—	1907.07	
Step 2	0–0.8076	16	2767.42	Total time of Step 2: 4958.92
	0.8076–1.4735	11	2191.50	
Total		27	6865.99	

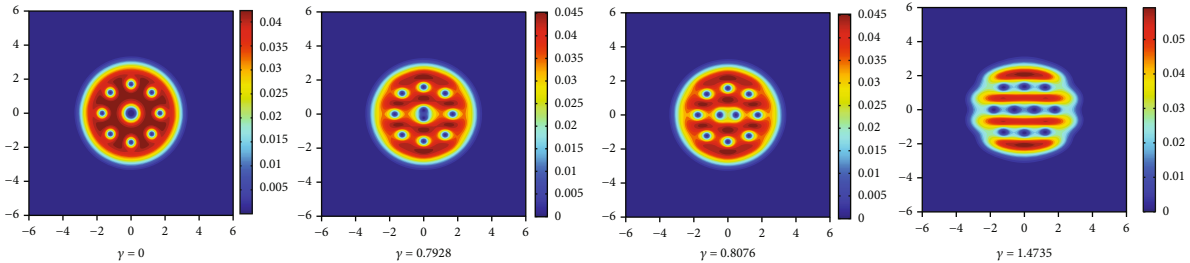


FIGURE 7: The contours of the ground state density function  $|\phi|^2$  of (15), where  $V_2(x, y) = (1.003x^2 + 0.997y^2)/2 + (1.003x^2 + 0.997y^2)^2/4$ ,  $\varepsilon = 1/\sqrt{5}$ ,  $\mathbf{n} = (1,0,1)/\sqrt{2}$ ,  $\omega = 1.9$ ,  $\beta = 500$ , and  $\lambda = \gamma\beta$ .

theoretically. However, when the wave function is obtained using numerical computation, we can compute all eigenvalues of (45) numerically and then discuss the linear stability of the wave function, see Example 4 for details.

## 5. Numerical Results

Algorithms 1 and 2 were implemented to compute the ground state solution of quasi-2D (rapidly) rotating dipolar BECs, where we used the SCM with  $N = 51$  (or  $N = 65$  for the rapidly rotating case) as the discretization method. In Examples 1–3, we chose  $V_2(x, y) = (1.003x^2 + 0.997y^2)/2$ ,  $\varepsilon$

$= 1/\sqrt{5}$ ,  $\omega = 0.9$  in (15), and the computational domain  $\Omega = (-12, 12)^2$ . The accuracy tolerance for the Newton corrector is  $5 \times 10^{-7}$ . We studied how the ground-state vortex structures were affected by the dipolar direction and the strength of the dipolar interaction. In Example 4, we discussed the linear stability analysis numerically. In Example 5, we considered the case of rapidly rotating dipolar BECs. All computations were executed on an Intel Core™ i7-2600K PC using Matlab language.

*Example 1.* We used Algorithm 1 to compute the ground state solution of quasi-2D rotating dipolar BECs (15) with

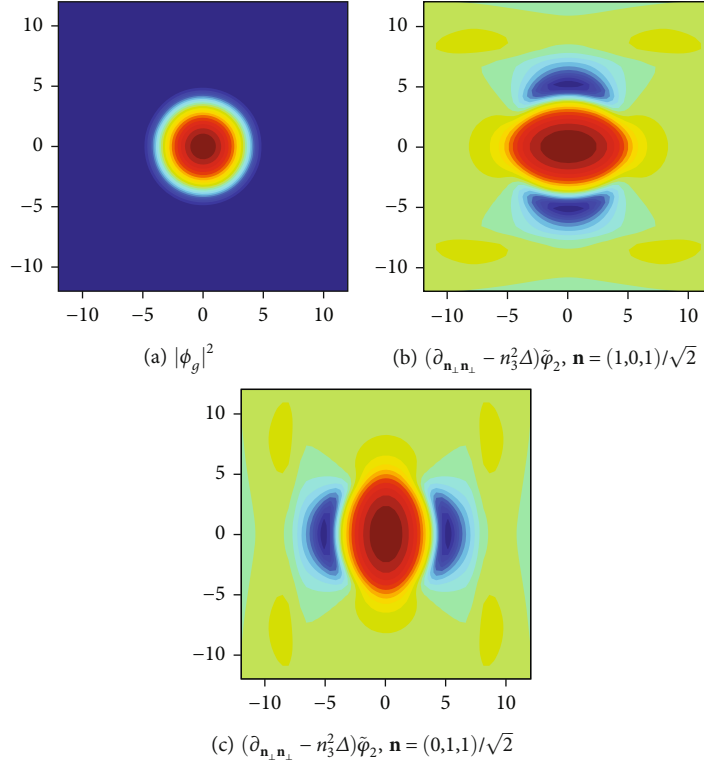


FIGURE 8: The contour of the density function  $|\phi_g|^2$  of the ground state of (15) with  $\omega = 0$  and  $\lambda = 0$ , and the contours of the function  $(\partial_{n_x n_x} - n^2 \Delta) \tilde{\varphi}_2$  corresponding to  $\phi_g$ .

$\mathbf{n} = (1,0,1)/\sqrt{2}$ ,  $\beta = 500$ , and  $\lambda = 200$ . We chose  $\tau_1 = 0.1$  and  $\tau_2 = 10^{-6}$  in Algorithm 1. Table 1 lists the implementation details, i.e., the first bifurcation points  $\mu_i$  and associated energy levels  $\mu_i^*$  of (15), the values of  $\|(\tilde{\varphi}_2)_{i,j} - (\tilde{\varphi}_2)_{i,j-1}\|_\infty$ , and the total execution time. Table 1 and Figure 1(a) show that we only need to trace the first solution curves twice, and the energy level of the ground state solution is  $\mu^* = 6.796239445$ . Figure 1(b) shows the contour plot of the density  $|\phi|^2$  for the ground state solution, where the hexagonal arrangement of the vortices is clearly visible. Figure 1(c) shows the phase of  $\phi$  for the ground state solution.

*Example 2.* Consider (15) with  $\mathbf{n} = (1,0,1)/\sqrt{2}$ ,  $\beta = 500$ , and  $\lambda = \gamma\beta$ . We implemented Algorithm 2 with  $\gamma_0 = 0$  and  $\gamma_{\text{end}} = 2.2$  to compute the ground state solution of (15). Figure 2(a) displays the solution curve of the wave function  $\phi$  in two-norm with respect to the chemical potential  $\mu$ . The blue solid line and the horizontal red dashed line were obtained by implementing Steps 1 and 2 of Algorithm 2, respectively. Note that in Step 2 of Algorithm 2, we can obtain the ground state solutions for various values of  $\gamma$ . Figure 2(b) depicts the relationship between  $\gamma$  and  $\mu$ . We observe that the chemical potential  $\mu$  increases almost linearly with respect to  $\gamma$ . Figure 3 displays the contours of the ground state density function  $|\phi|^2$  for  $\gamma = 0, 0.5123, 1.1017$ , and  $2.0856$ . From this figure, we can see that (i) when  $\gamma = 0$  (i.e., the dipolar interaction is absent), the vortex lattice forms a hexagonal structure. (ii) As the parameter  $\gamma$

increases, the number of vortices also increases and the vortices form straight lines that are parallel to the  $x$ -axis. Table 2 lists the execution time of implementing Algorithm 2 and the number of iterations in the while loop (NIW) of Step 2. The total NIW of 14 means that from  $\gamma = 0$  to  $\gamma = 2.0856$ , we obtain ground state solutions for 14 different values of  $\gamma$ . The average execution time for each value of  $\gamma$  is  $551.28/14 \approx 39.38$  seconds. Hence, using the ground state solution for  $\gamma = 0$  as the starting point, Step 2 of Algorithm 2 can effectively trace ground state solutions for other values of  $\gamma$ .

*Example 3.* We implemented Algorithm 2 to compute the ground state solution of (15) with  $\beta = 500$ ,  $\lambda = \gamma\beta$ , and two different dipolar directions  $\mathbf{n} = (0,1,1)/\sqrt{2}$  and  $\mathbf{n} = (1,1,1)/\sqrt{3}$ . Figure 4 shows the contours of the ground state density function  $|\phi|^2$  for some sample values of  $\gamma$ . From this figure, we can see that (i) as the parameter  $\gamma$  increases, the vortices form straight lines and then gradually pinned together to form vortex bands. (ii) For  $\mathbf{n} = (0,1,1)/\sqrt{2}$ , the vortex band orientation is parallel to the  $y$ -axis. (iii) For  $\mathbf{n} = (1,1,1)/\sqrt{3}$ , the vortex band orientation makes an angle of 60 degrees with the  $x$ -axis.

*Example 4 (linear stability analysis).* To study the linear stability of (11) numerically, we chose some data in Examples 2–3 and used the built-in function “eig” in Matlab to compute all eigenvalues of the corresponding equation (45). Figure 5 shows the discrete eigenvalues distribution of (45). From this figure, we can see that (i) when  $\omega = 0$ , there is

one eigenvalue with a positive real part. (ii) When the angular velocity  $\omega = 0.9$ , some eigenvalues of (45) have positive real parts. Therefore, in these cases, the discrete ground state solutions of (11) are linearly unstable.

*Example 5* (rapidly rotating dipolar BECs). In this example, we investigated how the ground-state vortex structures of rapidly rotating dipolar BECs were affected by  $\omega$ ,  $\mathbf{n}$ , and  $\lambda$ . To this end, we replaced the harmonic potential  $V_2(x, y) = (1.003x^2 + 0.997y^2)/2$  in (15) by the harmonic-plus-quartic potential [19, 26]

$$\tilde{V}_2(x, y) = \frac{(1.003x^2 + 0.997y^2)}{2} + \frac{(1.003x^2 + 0.997y^2)^2}{4}, \quad (48)$$

and set  $\varepsilon = 1/\sqrt{5}$ ,  $\beta = 500$ ,  $\lambda = \gamma\beta$ ,  $\Omega = (-6, 6)^2$ , and consider two cases:  $\omega = 1.7$  and  $\omega = 1.9$ .

(1)  $\omega = 1.7$ . Algorithm 2 with  $\gamma_0 = 0$  and  $\gamma_{\text{end}} = 1.65$  was implemented to compute the ground state solution of (15), where we considered two different dipolar directions: (a)  $\mathbf{n} = (1, 0, 1)/\sqrt{2}$  and (b)  $\mathbf{n} = (0, 1, 1)/\sqrt{2}$

(a)  $\mathbf{n} = (1, 0, 1)/\sqrt{2}$ . Figure 6(a) shows the contours of the ground state density function  $|\phi|^2$  for  $\gamma = 0, 0.3410, 0.7196, 1.1740$ , and  $1.6068$ . From this figure, we can see that (i) when  $\gamma = 0$  (i.e.,  $\lambda = 0$ ), six vortices are arranged in a hexagonal pattern. (ii) As the parameter  $\gamma$  increases, the vortices are gradually rearranged into two rows and form square lattices. And the orientation of the vortex lattice is parallel to the  $x$ -axis. Moreover, the number of vortices also evolves gradually from 6 to 10

(b)  $\mathbf{n} = (0, 1, 1)/\sqrt{2}$ . Figure 6(b) shows the contours of the ground state density function  $|\phi|^2$  for  $\gamma = 0, 0.3422, 1.0160, 1.3246$ , and  $1.6460$ . We observe that as the parameter  $\gamma$  increases, the vortices are gradually arranged in three columns. And in the middle column, the number of vortices evolves gradually from 2 to 4

(2)  $\omega = 1.9$ . Algorithm 2 with  $\gamma_0 = 0$  and  $\gamma_{\text{end}} = 1.5$  was implemented to compute the ground state solution of (15), where we chose  $\mathbf{n} = (1, 0, 1)/\sqrt{2}$ . The execution time of Algorithm 2 and the NIW of Step 2 are listed in Table 3. From this table, we observe that using the ground state solution for  $\gamma = 0$  as the starting point, Step 2 can effectively trace ground state solutions for other values of  $\gamma$ , and the average execution time for each value of  $\gamma$  is  $4958.92/27 \approx 183.66$  seconds. Figure 7 displays vortex lattice struc-

tures of the ground state for  $\gamma = 0, 0.7928, 0.8076$ , and  $1.4735$ . From this figure, we can see that (i) when  $\gamma = 0$ , one big vortex at the center is surrounded by eight small vortices in a ring. (ii) With the increasing of  $\gamma$ , the big vortex at the center is gradually split into two small vortices. (iii) When  $\gamma$  increases further, such as  $\gamma = 1.4735$ , the vortices are rearranged and aligned in three lines along the direction  $\mathbf{n}_\perp$

From Examples 2, 3, and 5, we observe that as the parameter  $\gamma$  increases, that is, as the strength of the dipolar interaction increases, the vortices gradually form some vortex bands parallel to the direction  $\mathbf{n}_\perp$ . This phenomenon is mainly related to the dipolar term  $-(3\lambda/2)(\partial_{\mathbf{n}_\perp \mathbf{n}_\perp} - n_3^2 \Delta)\tilde{\varphi}_2$  in (15), where  $\tilde{\varphi}_2 = U_2 * |\phi|^2$  involves the unknown wave function  $\phi$ . To understand the effect of this dipolar term on the vortex configuration, we take  $\phi = \phi_g$ , the ground state solution of (15) with  $\lambda = 0$ , and numerically compute the function  $(\partial_{\mathbf{n}_\perp \mathbf{n}_\perp} - n_3^2 \Delta)\tilde{\varphi}_2$ . Figure 8(a) depicts the contour plot of the density function  $|\phi_g|^2$  for  $\omega = 0$ , while Figures 8(b) and 8(c) depict the contour plots of the function  $(\partial_{\mathbf{n}_\perp \mathbf{n}_\perp} - n_3^2 \Delta)\tilde{\varphi}_2$  corresponding to  $\phi = \phi_g$  with  $\mathbf{n} = (1, 0, 1)/\sqrt{2}$  and  $(0, 1, 1)/\sqrt{2}$ , respectively. We can see that the contour plot of the function  $(\partial_{\mathbf{n}_\perp \mathbf{n}_\perp} - n_3^2 \Delta)\tilde{\varphi}_2$  is an ellipse whose minor axis is perpendicular to the direction  $\mathbf{n}_\perp$ . This means that the dipolar term is anisotropic even though the density wave function  $|\phi_g|^2$  is isotropic. Hence, as the strength of the dipolar interaction increases, the condensates will be squeezed in the direction perpendicular to  $\mathbf{n}_\perp$ . Due to this squeezing, the vortices will be rearranged and aligned parallel to the direction  $\mathbf{n}_\perp$ . Our numerical results confirm this phenomenon.

## 6. Conclusions

We have presented an efficient two-parameter continuation algorithm for computing the ground state solution of quasi-2D (rapidly) rotating dipolar BECs, where the SCM was used to discretize the corresponding GPE. The main advantage of this algorithm is that we only need to trace the solution curve once to obtain various ground state solutions associated with different strengths of the dipolar interaction. Thus, the change of the ground-state vortex structure with increasing the dipolar interaction strength can be easily observed. In addition, we have also studied linear stability analysis for the ground state of rotating dipolar BECs. Based on the numerical experiments reported in Section 5, we may give some concluding remarks as follows: (i) the ground-state vortex structure of rotating dipolar BECs is affected by the strength of the dipolar interaction and the dipolar direction. More specifically, as the strength of the dipolar interaction increases, the vortices are gradually aligned in lines along the dipolar direction. When the strength is large enough, some vortices on the vortex lines are pinned together to form vortex bands. Moreover, for the rapidly rotating case, we also observe that the big vortex at the

center is gradually split into two small vortices with increasing the dipolar interaction. (ii) In Example 4, we have shown numerically that the discrete ground state solutions of quasi-2D dipolar BECs are linearly unstable, both with and without rotating term.

### Data Availability

The data used to support the findings of this study are included within the article.

### Conflicts of Interest

The authors declare that there are no conflicts of interest regarding the publication of this paper.

### Acknowledgments

This study was funded by Ministry of Science and Technology of R.O.C. (Taiwan) (MOST 103-2115-M-142-003).

### References

- [1] A. Griesmaier, J. Werner, S. Hensler, J. Stuhler, and T. Pfau, "Bose-Einstein condensation of chromium," *Physical Review Letters*, vol. 94, no. 16, article 160401, 2005.
- [2] M. Lu, N. Q. Burdick, S.-H. Youn, and B. L. Lev, "Strongly dipolar Bose-Einstein condensate of dysprosium," *Physical Review Letters*, vol. 107, no. 19, article 190401, 2011.
- [3] K. Aikawa, A. Frisch, M. Mark et al., "Bose-Einstein condensation of erbium," *Physical Review Letters*, vol. 108, no. 21, article 210401, 2012.
- [4] T. Lahaye, J. Metz, B. Frohlich et al., "d-Wave collapse and explosion of a dipolar Bose-Einstein condensate," *Physical Review Letters*, vol. 101, no. 8, article 080401, 2008.
- [5] L. Santos, G. V. Shlyapnikov, and M. Lewenstein, "Roton-Maxon spectrum and stability of trapped dipolar Bose-Einstein condensates," *Physical Review Letters*, vol. 90, no. 25, article 250403, 2003.
- [6] R. M. Wilson, S. Ronen, J. L. Bohn, and H. Pu, "Manifestations of the roton mode in dipolar Bose-Einstein condensates," *Physical Review Letters*, vol. 100, no. 24, article 245302, 2008.
- [7] M. Schmitt, M. Wenzel, F. Böttcher, I. Ferrier-Barbut, and T. Pfau, "Self-bound droplets of a dilute magnetic quantum liquid," *Nature*, vol. 539, no. 7628, pp. 259–262, 2016.
- [8] L. Chomaz, S. Baier, D. Petter et al., "Quantum-fluctuation-driven crossover from a dilute Bose-Einstein condensate to a macrodroplet in a dipolar quantum fluid," *Physical Review X*, vol. 6, no. 4, article 041039, 2016.
- [9] L. Tanzi, E. Lucioni, F. Famá et al., "Observation of a dipolar quantum gas with metastable supersolid properties," *Physical Review Letters*, vol. 122, no. 13, article 130405, 2019.
- [10] M. Klawunn, R. Nath, P. Pedri, and L. Santos, "Transverse instability of straight vortex lines in dipolar Bose-Einstein condensates," *Physical Review Letters*, vol. 100, no. 24, article 240403, 2008.
- [11] D. H. O'Dell and C. Eberlein, "Vortex in a trapped Bose-Einstein condensate with dipole-dipole interactions," *Physical Review A*, vol. 75, no. 1, article 013604, 2007.
- [12] S. Yi and H. Pu, "Vortex structures in dipolar condensates," *Physical Review A*, vol. 73, no. 6, article 061602, 2006.
- [13] W. Bao, Y. Cai, and H. Wang, "Efficient numerical methods for computing ground states and dynamics of dipolar Bose-Einstein condensates," *Journal of Computational Physics*, vol. 229, no. 20, pp. 7874–7892, 2010.
- [14] Y. Cai, M. Rosenkranz, Z. Lei, and W. Bao, "Mean-field regime of trapped dipolar Bose-Einstein condensates in one and two dimensions," *Physical Review A*, vol. 82, no. 4, article 043623, 2010.
- [15] W. Bao, N. B. Abdallah, and Y. Cai, "Gross-Pitaevskii-Poisson equations for dipolar Bose-Einstein condensate with anisotropic confinement," *SIAM Journal on Mathematical Analysis*, vol. 44, no. 3, pp. 1713–1741, 2012.
- [16] B.-W. Jeng, C.-S. Chien, and I.-L. Chern, "Spectral collocation and a two-level continuation scheme for dipolar Bose-Einstein condensates," *Journal of Computational Physics*, vol. 256, pp. 713–727, 2014.
- [17] W. Bao, Q. Tang, and Y. Zhang, "Accurate and efficient numerical methods for computing ground states and dynamics of dipolar Bose-Einstein condensates via the nonuniform FFT," *Communications in Computational Physics*, vol. 19, no. 5, pp. 1141–1166, 2016.
- [18] X. Antoine, Q. Tang, and Y. Zhang, "A preconditioned conjugated gradient method for computing ground states of rotating dipolar Bose-Einstein condensates via kernel truncation method for dipole-dipole interaction evaluation," *Communications in Computational Physics*, vol. 24, pp. 966–988, 2018.
- [19] B.-W. Jeng, Y.-S. Wang, and C.-S. Chien, "A two-parameter continuation algorithm for vortex pinning in rotating Bose-Einstein condensates," *Computer Physics Communications*, vol. 184, no. 3, pp. 493–508, 2013.
- [20] S.-L. Chang and C.-S. Chien, "Adaptive continuation algorithms for computing energy levels of rotating Bose-Einstein condensates," *Computer Physics Communications*, vol. 177, no. 9, pp. 707–719, 2007.
- [21] H.-S. Chen, S.-L. Chang, and C.-S. Chien, "Spectral collocation methods using sine functions for a rotating Bose-Einstein condensation in optical lattices," *Journal of Computational Physics*, vol. 231, no. 4, pp. 1553–1569, 2012.
- [22] S.-Y. Chen, Y.-S. Wang, B.-W. Jeng, and C.-S. Chien, "Multi-parameter continuation and collocation methods for rotating multi-component Bose-Einstein condensates," *International Journal of Computer Mathematics*, vol. 92, no. 4, pp. 850–871, 2015.
- [23] H.-S. Chen, S.-L. Chang, B.-W. Jeng, and C.-S. Chien, "Continuation and stability analysis for Bloch waves of the Gross-Pitaevskii equation," *Numerical Algorithms*, vol. 77, no. 3, pp. 709–726, 2018.
- [24] B. Wu and Q. Niu, "Superfluidity of Bose-Einstein condensate in an optical lattice: Landau-Zener tunnelling and dynamical instability," *New Journal of Physics*, vol. 5, pp. 104.1–104.24, 2003.
- [25] J. Yang, *Nonlinear Waves in Integrable and Nonintegrable Systems*, SIAM, Philadelphia, 2010.
- [26] A. L. Fetter, B. Jackson, and S. Stringari, "Rapid rotation of a Bose-Einstein condensate in a harmonic plus quartic trap," *Physical Review A*, vol. 71, no. 1, article 013605, 2005.